Theoretical de Haas-van Alphen Data and Plasma Frequencies of MgB_2 and TaB_2

S. Elgazzar[1], P.M. Oppeneer, S.-L. Drechsler, R. Hayn, H. Rosner[†]
Institut für Festkörper- und Werkstofforschung, P.O. Box 270116, D-01171 Dresden, Germany
[†]*Dept. of Physics, University of California, Davis CA 95616, USA*

The de Haas-van Alphen-frequencies as well as the effective masses for a magnetic field parallel to the crystallographic c-axis are calculated within the local spin density approximation (LSDA) for MgB_2 and TaB_2. In addition, we analyze the plasma frequencies computed for each Fermi surface sheet. We find a large anisotropy of Fermi velocities in MgB_2 in difference to the nearly isotropic behavior in TaB_2. We compare calculations performed within the relativistic non-full potential augmented-spherical-wave (ASW) scheme and the scalar-relativistic full potential local orbital (FPLO) scheme. A significant dependence for small cross sections on the bandstructure method is found. The comparison with the first available experimental de Haas-van Alphen-data by Yelland *et al.* (Ref. 19) shows deviations from the electronic structure calculated within both L(S)DA approaches although the cross section predicted by FPLO are closer to the experimental data. The elucidation of the relevant many-body effects beyond the standard LDA is considered as a possible key problem to understand the superconductivity in MgB_2.

71.18.+y; 74.70.Ad; 74.25.Jb

I. INTRODUCTION

The unexpected discovery of superconductivity in MgB_2[1], with a surprisingly high transition temperature $T_c \sim 40$ K, has raised considerable interest in the clarification of its electronic structure and its relationship to the mechanism of superconductivity. The present theoretical approaches to this challenging problem can be divided roughly into three scenarios emphasizing: (i) a conventional electronic structure and a more or less standard electron-phonon interaction within a (multiple) wide-band model[2−7], (ii) the presence of strong electron-electron[8] or magnetic interactions[9], and (iii) strong nonadiabatic[10] or polaronic[11] effects. In the present paper we shall mainly consider the first approach which is based on calculations of the electronic structure within the local (spin) density approximation (L(S)DA) to the density-functional theory. The L(S)DA band structure calculations[2−7] revealed four sheets of the Fermi surface of MgB_2 with a remarkable high anisotropy of Fermi velocities for σ-holes. That anisotropy is important to explain the significant anisotropy of the upper critical field $H_{c2}(T)$ in terms of a two-band Eliashberg model[5−7]. The relatively high value of $H_{c2}(0)$ is related to the strong electron-phonon interaction of the σ-holes on the tube-like Fermi surface sheets[7]. Details of the electronic structure are important for a precise understanding of the pairing mechanism, like, e.g., by comparing the calculated "undressed" electronic effective mass with its actual dressed value due to the electron-phonon coupling. On the other hand, it is interesting to compare MgB_2 with related isostructural compounds having much lower transition temperatures or even showing no superconductivity at all. We choose here TaB_2 for which band structure calculations have been reported recently [12−14] and for which single crystals can be produced[15]. It should be noted that stochiometric TaB_2 is non-superconducting (at least down to 1.5 K[12,16,17]) and another phase, unidentified yet, should be responsible for the observed superconductivity with a T_c of 9.5 K[18].

II. METHODS

Very detailed insight into the electronic structure can be gained from de Haas-van Alphen (dHvA) measurements. To the best of our knowledge there is as yet only one very recent measurement devoted to MgB_2[19] and we are not aware of any dHvA-experiments for TaB_2. With the aim to initiate possible experiments, we provided calculated dHvA-frequencies and effective masses for the two materials under consideration[20]. From that data one can extract information about the Fermi velocities averaged over the extremal orbits. We discuss also the possible enhancement of the effective masses by the electron-phonon coupling which is expected to be quite different for the two materials. Information about the Fermi velocities can furthermore be obtained by means of the plasma frequencies detectable from the Drude part of the optical conductivity. We compare also the plasma frequencies computed for each Fermi surface sheet and find a large amount of anisotropy in MgB_2 in difference to TaB_2.

The band structure calculations have been performed by means of two computational codes: (i) the fully relativistic augmented spherical waves method (ASW)[21] and (ii) the scalar relativistic full potential local orbital scheme (FPLO). In case (i) we used the von Barth-Hedin parametrization of the exchange-correlation potential. A k-mesh of 148 special k-points in the irre-

ducible Brillouin zone part was chosen. For details of case (ii) see e.g. Ref.[7,12].

Both compounds crystallize in the hexagonal space group $P6/mmm$ with lattice constants $a = 3.083$ Å, $c = 3.5208$ Å and $a = 3.082$ Å, $c = 3.243$ Å[18] for MgB_2 and TaB_2, respectively. The resulting ASW band structure for MgB_2 is similar with those published in the literature[2−7] and it is shown for the sake of completeness in Fig. 1. The relativistic band structure of TaB_2 is presented in Fig. 2. We have checked our results by comparing them with the scalar relativistic full-potential local orbital (FPLO) method repeating previous calculations (MgB_2[5−7], TaB_2[12]) and we found some differences for both compounds. In MgB_2 these differences are not

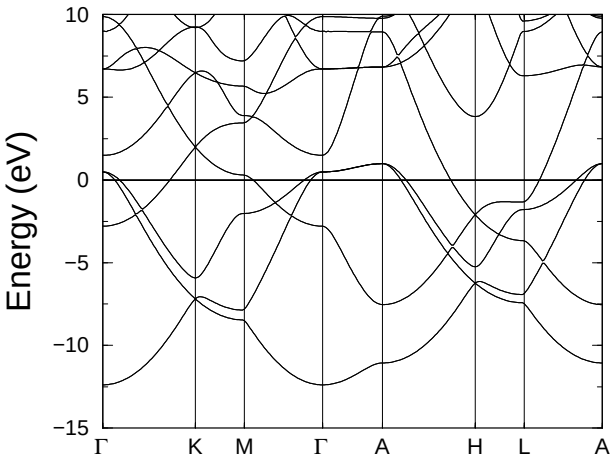

FIG. 1. The calculated energy bands of MgB_2. The Fermi energy is at zero energy.

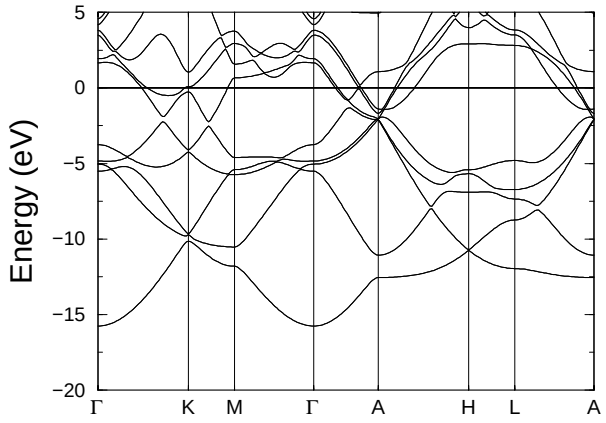

FIG. 2. The same as in Fig. 1 for TaB_2.

due to the spin-orbit coupling in a fully relativistic calculation. Instead we are forced to ascribe these effects mainly to a slightly different crystal field potential in spherical or full-potential descriptions, which affects the relative position of boron derived π and σ bands. The spin-orbit coupling of the Ta $5d$ states in TaB_2 results in differences compared to scalar relativistic calculations, especially between Γ and A (compare Fig. 2 and Fig. 3 of Ref. 12). Although these differences should not affect the absence of superconductivity in this compound, they lead to consequences for the Fermi surface to be discussed below. To predict the dHvA-frequencies F for a magnetic field applied, say along the crystallographic $\vec{c}$ direction, we calculate the area A of any extremal orbit Ω according to the Onsager relation (written in cgs units)

$$F = \frac{\hbar c}{2\pi e} A = \frac{\hbar c}{2\pi e} \int_\Omega d^2k \quad . \tag{1}$$

It is convenient to measure F in units of the applied magnetic field and A in units of squared wave vectors, e.g., in kT (1kT=10^7G) and the cross-section A in nm^{-2}, respectively. Then Eq. (1) reads simply

$$F = 0.104867 \times A \quad . \tag{1'}$$

The effective mass of the corresponding orbit is given by

$$m = \frac{\hbar}{2\pi} \oint \frac{dk}{|\vec{v}_k|}, \qquad \text{with} \qquad \vec{v}_k = \frac{\partial \epsilon_k}{\partial \vec{k}}. \tag{2}$$

From the dHvA-frequency F and the effective mass m one can introduce an effective Fermi velocity

$$v_f = \frac{\hbar}{m}\sqrt{\frac{A}{\pi}} = \frac{1}{m}\sqrt{\frac{2\hbar e F}{c}}, \tag{3}$$

which corresponds to the hypothetical value for a circular orbit with constant $|\vec{v}_{\vec{k}}|$. This expression is frequently used to estimate the Fermi velocity from dHvA data. Alternatively, one can also average $1/|\vec{v}_k|$ around the circumference and define

$$\tilde{v}_f = \frac{\hbar L}{2\pi m} = \frac{\hbar}{2\pi m} \oint dk. \tag{4}$$

Obviously, both velocities defined by Eqs. (3) and (4) coincide for a circular orbit. For an orbit with an ideal hexagon shape $v_f/\tilde{v}_f = \sqrt{\pi/2\sqrt{3}} \approx 0.9523$ is estimated from Eqs. (2,3). Both of these quantities contain averages of point properties of the Fermi surface around a cyclotron orbit.

Information about the Fermi velocity is also contained in the plasma frequencies $\omega_{p,\alpha}$ ($\alpha = x(y)$ or z)

$$(\omega_{p,\alpha})^2 = \frac{e^2}{\epsilon_\circ} \int \frac{d^3k}{(2\pi)^3} \delta(\epsilon_k - E_f)(v_{k,\alpha})^2, \tag{5}$$

where we will distinguish the contributions from different Fermi surface sheets in the following (denoted by $\omega^n_{p,\alpha}$).

Analogously to Eq. (5), components α of the Fermi velocities $v_\alpha = \sqrt{< v_\alpha^2 >_{FS}}$ can be introduced which are averaged over selected sheets or over the whole Fermi surface (FS)

$$(v_\alpha)^2 = \int \frac{d^3k}{(2\pi)^3} \delta(\epsilon_k - E_f)(v_{k,\alpha})^2. \qquad (6)$$

The ratio of these Fermi velocity components related to the most anisotropic σ-tubes with the strongest el-ph interaction at the same time can be used to describe upper bounds for the anisotropy parameter γ of the upper critical field H_{c2},

$$\gamma = H_{c2}^{ab}/H_{c2}^{c} < \sqrt{< v_{f,xy}^2 >_{tubes} /2 < v_{f,z}^2 >_{tubes}} \quad ,$$

if that anisotropy is the predominant one as suggested by several microscopic calculations[5].

III. MAGNESIUM DIBORIDE

Let us first discuss the results for MgB_2. The band structure near the Fermi energy E_f is depicted in Fig. 1. The corresponding dHvA-data for a magnetic field directed along the c-axis are shown in Table I. (Note that in our previous paper[20] the numbers for the orbits 2 and 4 were mistakenly interchanged.) The Fermi surface of

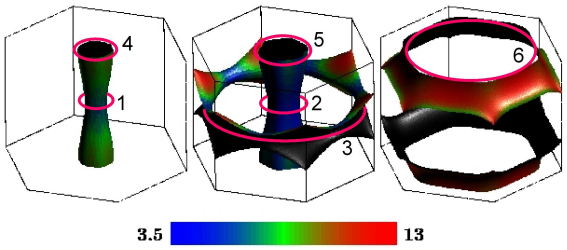

FIG. 3. (Color) The calculated Fermi surface, distribution of Fermi velocities, and extremal orbits (pink lines, the numbers denote the orbits that are explained in the text) (magnetic field $\parallel$ c-axis) of MgB_2. The Fermi velocities expressed by different colors (blue-slow, green-medium, read-fast) are given in units of 10^5m/s as shown in the legend.

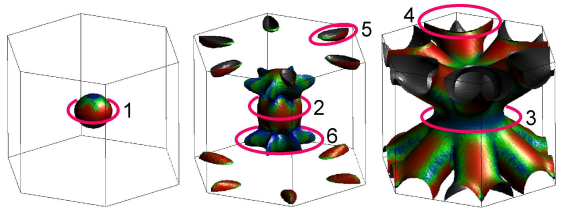

FIG. 4. (Color) The same as in Fig. 3 for TaB_2. Note that for visibility purposes A is at the center of the hexagonal prism and the Γ point is the midpoint of the lower and the upper hexagon.

MgB_2 (see Fig. 3) consists of four sheets and there are 6 extremal orbits for a magnetic field in $\vec{c}$ direction. We will denote them by numbers 1 to 3 centered around Γ and 4 to 6 centered around A with increasing area in each case. So one can see that orbits 1 and 4 (2 and 5) belong to the smaller (larger) tube, where the remaining orbits 3 and 6 are rather large and belong to the ring-like parts of the Fermi surface. The electrons on orbit 6 have the largest Fermi velocity and v_f of orbit 3 is smaller compared to that of orbit 6 due to the larger effective mass. The electrons on the tubes are slow in general, with the minimal velocity on orbit 2. The ratio of Fermi velocities for the two different groups of electrons is roughly 2. In addition there is a rather different strength of the electron-phonon interaction on both types of Fermi surface sheets: strong on the tubes and weak on π-derived rings. This confirms the introduction of a two-band model proposed for MgB_2 first by Shulga *et al.*[6] and elaborated later on in Ref. 22.

The relative difference $(v_f - \tilde{v}_f)/v_f$ does not exceed 7 percent and it is noteworthy only for those orbits which have a pronounced hexagonal form than a nearly circular one (for example orbit 3 is such a nearly circular orbit). According to the two-band model[6] we would expect a different electron-phonon mass renormalization $(1+\lambda)$ for electrons on the tubes (with $\lambda \simeq 1.2 \cdots 1.5$) and on the large orbits 3 and 6 ($\lambda \simeq 0.3$). The comparison with the experimentally determined cross sections shows significant deviations from our L(S)DA predictions. The microscopic reason for that unexpected deviation remains unclear at the moment. Standard electron-phonon interaction does not affect the cross-section. It might explain only the renormalization of the Fermi velocities and of the masses. The cross-sections might be affected by strong electron-electron interaction and/or the presence of electronic instabilities competing with superconductivity which might result in local changes (destruction) of the Fermi surface by a partial dielectrization (gapping) from a charge density or spin density wave[23]. The experiments yield a much narrower smaller tube than the L(S)DA calculation predict. While this already indicates a discrepancy between theory and experiment, more serious might be the fact that the wider, second tube is not observed in the experiment at all. Would this fact be confirmed also for cleaner samples, i.e. the missing cross sections with lower Fermi velocities could not be attributed to the residual impurity scattering[19], it would imply the failure of the L(S)DA to describe correctly MgB_2.

We consider the elucidation of the responsible many-body effects which are missing in the standard LDA approach to MgB_2, i.e. treating it as a simple sp-metal, as a possible key problem for our physical understanding of the electronic structure of MgB_2 and its remarkable superconductivity as well. Anyhow, in view of the great importance of the experimental dHvA data, the confirmation of a more or less unusual electronic structure in MgB_2 by other groups using different single crystals would be highly desirable.

The experimental determination of the effective

masses by dHvA measurements and its comparison with the calculated electronic values gives important information on details of the electron-phonon coupling. If the assignment proposed in Ref. 19 is correct, strongly renormalized Fermi velocities by a factor of 2 to 3 should be explained. Comparing the calculated and measured masses for the smaller tube, one arrives at a slightly larger local $\lambda \approx 1.27$ compared with $\lambda \approx 1$ obtained by Choi *et al.*[22] within full anisotropic (harmonic) Eliashberg theory.

If the corresponding coupling constant for the larger tube would be also enhanced, possible contributions from the coupling of a soft mode should be considered. Otherwise it would be unclear, why for a non-enhanced Coulomb repulsion (measured by the Coulomb pseudopotential μ^*) or the absence of any other enhanced pair-breaking, the critical temperature is not higher than 40 K. In this context the recent experimental observation of a soft-mode near 17 meV in Raman spectroscopy[24], point contact spectroscopy[25] as well as in neutron scattering[26] is of considerable interest. Especially with respect to the assignment of that boson-mode, since standard harmonic phonon calculations are unable to explain the presence of such a low-lying mode[4]. Notably, also from recent standard tunneling experiments[27] (unfortunately with a cut off at 26 meV, i.e. just slightly above the low-frequency anomalies) significant deviations from the standard harmonic phonon calculations have been reported.

The anisotropy of Fermi velocities of MgB_2 is even more visible in our calculated plasma frequencies (see Table II), which are similar to the results of Refs. 4,3,28,29 (see Table III). In our previous calculation[20] a scaling factor of c/a was missing for $\omega_{px(y)}$. Here we have corrected the present results for that factor. It is another kind of anisotropy: the z-component of v_f is about 6 times smaller than the *x(y)* components for the two tubes (sheets 1 and 2). The anisotropy ratio $v^n_{p,x(y)}/v^n_{p,z}$ ($v^n_\alpha \propto |\omega^n_{p,\alpha}|$) is much smaller for the sheets 3 and 4 and its average Fermi velocity is larger. The total plasma frequency, however, shows only a small anisotropy of 1.04 between the z and *x(y)* components. In Table III we compare the anisotropy in the components of the total plasma frequency as obtained by various groups. The obtained numbers are generally in good agreement with one another.

The anisotropy of Fermi velocities is much less pronounced in TaB_2 (Tables III and IV). Our fully relativistic Fermi surface coincides almost with that published in[12] and consists of three sheets. The extremal orbits are characterized as follows (s. Fig. 3): numbers 1 to 3 are centered around the A point and correspond to the three different sheets. Orbit 4 is centered around K and orbit 5 corresponds to the small Fermi surface part in the neighborhood of K. There is one maximal orbit (number 6) with nontrivial value k_z ($0.20615 \times 2\pi/a$). Since Ta is a $5d$ element, the influence of the spin-orbit coupling is more pronounced in TaB_2 than in MgB_2. With respect to the scalar relativistic calculations[12] we find two differences that affect the Fermi surface: First, a splitting of bands along the high symmetry direction $\Gamma - A$, which leads to a lifting of band degeneracy at the Fermi level. Second, also at the K-point a small band shift occurs. The first spin-orbit modification of the Fermi surface makes one Fermi sheet disjointed along $\Gamma - A$. The calculated areas, effective masses and Fermi velocities of TaB_2 are collected in Table IV and one can see that any kind of anisotropies of Fermi velocities is much smaller than for MgB_2. According to the calculation of the electron-phonon coupling constants[12] we would expect a rather small renormalization of effective masses in TaB_2 ($\lambda \simeq 0.05 \cdots 0.2$) again in difference to MgB_2. The plasma frequencies are collected in Table V. Since there are no analogous FS sheets to the two tubes of MgB_2 we do not obtain a corresponding anisotropy in $\omega^n_{p,x(y)}$ with respect to $\omega^n_{p,z}$. This can be understood due to the loss of the quasi two-dimensionality of the B σ-states in TaB_2 due to the hybridization with the Ta $5d$ states.

The hole Fermi sheet around A shown in the middle panel of Fig. 4 resembles a feature calculated within an augmented-plane-wave code for ZrB_2[30] The experimentally observed dHvA-frequencies of the central ε-orbit[31] (corresponding to orbit No. 2 in Fig. 4) near 1.8 kT and 1.5 kT for the similar system TiB_2[32], respectively, are significantly smaller than 3.48 kT in our FPLO-calculation for TaB_2. The opposite behaviour is observed for the $\mu-$orbit (orbit No. 6 in Fig. 4) where the experimental values for ZrB_2 and TiB_2 read 2.46 kT and 3.44 kT compared with our FPLO calculated 3.44 kT for TaB_2. Further theoretical and experimental studies should be awaited to answer the important question whether there are significant deviations even from full-potential L(S)DA-calculations only for the peculiar MgB_2 or also for other diborides with weak electron-phonon interaction.

IV. SUMMARY AND CONCLUSIONS

In summary, we have calculated the dHvA-frequencies and effective masses as well as the plasma frequencies of MgB_2 and TaB_2 which would be worth to be investigated experimentally in detail. First experimental de Haas-van Alphen data for MgB_2 point to significant deviations. The comparison of the experimental masses with L(S)DA calculation could give important information on the electron-phonon coupling. According to Refs.[2,7,12] we expect remarkable differences between MgB_2 and TaB_2: Large enhancement for one group of electrons in MgB_2 and a small enhancement for the other electrons in MgB_2 as well as in TaB_2. We found a remarkable anisotropy of Fermi velocities in superconducting MgB_2 which is in difference to the more isotropic behavior of non-superconducting TaB_2.

*Note added.*After finishing the present second version of our work we have learnt on a closely related work by

Mazin and Kortus[33] who also stress the necessity of full-potential calculations for MgB_2 and arrive essentially at very close numerical values for the cross sections and the masses under consideration (see Table I). Remaining slight numerical differences, comparison with other full-potential bandstructure codes, and somewhat different physical interpretation will be discussed elsewhere[34].

ACKNOWLEDGMENTS

We thank S.V. Shulga, I. Mazin, and A. Carrington for critical remarks and discussions. We are indebted to H. Eschrig, M. Richter, V.D.P. Servedio, W. Pickett and J. An for discussions. This work was supported by the Egyptian Ministry of Higher Education and Scientific Research and by the DAAD (individual grant to H.R.), ONR Grant No. N00017-1-0956 and the DFG, SFB 463.

---

[1] On leave from Faculty of Science, Menoufia University, Shebin El-Kom, Egypt

---

[1] Nagamatsu, J., Nakagawa, N., Muranaka, T., Zenitani, Y., and Akimitsu, J., *Nature* **410**, 63-64 (2001).

[2] An, J.M., and Pickett, W.E., *Phys. Rev. Lett.* **86**, 4366 (2001).

[3] Kortus, J., Mazin, I.I., Belashchenko, K.D., Antropov, V.P., and Boyer, L.L., *Phys. Rev. Lett.* **86**, 4656 (2001); Liu, A.Y., Mazin, I.I., and Kortus, J., *Phys. Rev. Lett.* **87**, 087005 (2001).

[4] Kong,Y., Dolgov, O.V., Jepsen, O., and Andersen, O.K., *Phys. Rev. B* **64**, 020501-020505 (2001).

[5] Fuchs, G., Drechsler, S.-L., Shulga, S.V., Müller, K.-H., Handstein, A., Nenkov, K., and Rosner, H., in *Studies of High-Temperature Superconductors-2001*, vol. 41, ed. A. Narlikar, Nova Science Publishers Inc., Commack, New York, (2001), (in press).

[6] Shulga, S.V., Drechsler, S.-L., Eschrig, H., Rosner, H., and W.E. Pickett, *cond-mat/* 0103154.

[7] Rosner, H., An, J.M., Ku, W., Johannes, M.D., Scalettar, R.T., Pickett, W.E., Shulga, S.V., Drechsler, S.-L., Eschrig, H., Weber, W., and Eguiluz, A.G., in *Studies of High-Temperature Superconductors*, vol. **38**, edited by A. Narlikar, Nova Science Publishers Inc., Commack, New York, 2001, (in press).

[8] Hirsch, J.E., and Marsiglio, F., *Phys. Rev.* **64**, 14 523 (2001), and *ibid* (2001).

[9] Imada M., *J. Phys. Soc. Jpn.* **70**, 1218 (2001); Furukawa, N., *cond-mat/*0103184.

[10] Boeri L., Bachelet, G.B., Cappelluti, E., and Pietronero, L., *cond-mat/*0112075 (2001); Cappelutti, E., Ciuchi, S., Grimaldi, C., Pietronero, L., and Strässler, S., *cond-mat/*0105351.

[11] Alexandrov, A., *cond-mat/*0103006.

[12] Rosner, H., Pickett, W.E, Drechsler, S.-L., Handstein, A., Behr, G. Fuchs, G., Nenkov, K., Müller, K.-H., and Eschrig, H., *Phys. Rev. B* **64**, 144516 (2001).

[13] Stein, I.R., and Ivanovski, A.L., *cond-mat/*0109445.

[14] Singh, P.P., *cond-mat/*0104580 .

[15] Otani, S., Korsukova, M.M., and Miksuhashi, T., *J. of Crystal Growth* **194**, 430-433 (1998).

[16] Leyarovska, L., and Leyarovska, E., *J. Less Common Metals* **67**, 249 (1979).

[17] Gasparov, V.A., Sidorov, N.S., Zvor'kova, I.L., and Kulakov, M.P., *JETP Letters* **73**, 532 (2001).

[18] Kaczorowski, D., Zaleski, A.J., Zogal, O.J., and Klamut, J., *cond-mat/*0103571.

[19] Yelland, E.A., Cooper, J.R., Carrington, A. Hussey, N.E., Meeson, P.J., Lee, S., Yamomoto A., and Tajima, S., *cond-mat/*0112392.

[20] Elgazzar, S., Oppeneer, P.M., Drechsler, S.-L., Hayn, R., and Rosner H., *Solid State Commun.* **121**, 99 (2002).

[21] Williams, A.R., Kübler, J., and Gelatt, C.D., *Phys. Rev. B* **19**, 6094 (1979).

[22] Choi, H.J., Roundy, D., Sun, H., Cohen, M.L., and Louie, G., *cond-mat/*0111182.

[23] Hase, I., and Yamaji, K.,*J. Phys. Soc. Jpn.***70**, 2376 (2001).

[24] Lampakis, D., Tatsi, A., Liarokapis, E., Varelogiannis, G., Oppeneer, P.M., Pissas, M., and Nishizaki, T., *cond-mat/*0105447.

[25] Bobrov, N.L., Chubov, P.N., Naidyuk, Yu.G., Trunina, L.V., and Yanson, I.K., *cond-mat/*0110006.

[26] Muranako, T., Margadonna, S., Maurin, I., Brigatti, K., Colgnesi, D., Prassides, K., Iwasa Y., Arai, M., Takata, M., Akimitsu, J., *J. Phys. Soc. Jpn.* **70**, 1480 (2001); Sato T.J., *et al. cond-mat/*0102468 (2001).

[27] D'yachenko, A.I., Tarenkov, V.Yu., Abal'oshev, A.V., and Lewandowski, S.J., *cond-mat/*0201200.

[28] Ravindran, P., Vajeeston, P., Vidya, R., Kjekshus, A, and Fjellvag, H., *cond-mat/*0104253.

[29] Singh, P.P., *cond-mat/*0104580.

[30] Ihara, H., Hirabayashi, M., and Nakagawa, H., *Phys. Rev. B* **16** 726-730 (1977).

[31] Tanaka, T., Ishizawa, Y., Bannai, E., and Kawai, S., *Solid Sate Comm.* **26** 879-882 (1978).

[32] Isizawa, Y., and Tanaka, T., *Inst. Phys. Conf. Ser. No. 75 Chapt. 1* 29-43 (1986).

[33] Mazin, I.I., and Kortus, J., *cond-mat/*0201247.

[34] Rosner, H., *et al.* in preparation.

TABLE I. The LSDA de Haas-van Alphen data of MgB_2 (magnetic field $\parallel c-$ axis). Available experimental values according to the assignment of Ref. 19 have been added for the sake of comparison. Calculated quantitities without explicit label have been computed within the ASW scheme.

orbit	F_{ASW}	F_{FPLO}	F_{exp}	A/A_{BZ}	$m/m_\circ$	$m_{exp}/m_\circ$	v_f	$v_{f,exp}$	$\tilde{v}_f$
	[kT]	[kT]	[KT]	%			[10^5m/s]	[10^5m/s]	[10^5m/s]
1	0.99	0.79	0.54	1.98	0.25	0.57	7.9	3.2	8.5
2	2.16	1.63		4.3	0.55		5.4		5.8
3	32.88	34.2		65.6	1.70		6.8		7.2
4	2.31	1.84	1.53	4.6	0.31	0.70	9.8	3.3	10.5
5	4.31	3.44		8.6	0.61		6.8		7.3
6	30.20	30.6		60.2	0.92		12.		12.8

TABLE II. Squared plasma frequencies of MgB_2 in [eV^2]. One eV for the plasma frequencies corresponds to 80.4· km/s.

FS sheet	$\omega^2_{p,x(y)}$	$\omega^2_{p,z}$	$v_{x(y)}/v_z$
1 (tube)	9.639	0.242	6.31
2 (tube)	9.444	0.323	5.40
3 (ring)	8.620	22.053	0.63
4 (ring)	23.042	24.6698	0.97
All	50.75	47.290	1.04

TABLE III. Comparison of several calculated results for the two components of the total plasma frequency ω_{px} and ω_{pz} of MgB_2 (in eV).

$\omega_{p,x(y)}$	$\omega_{p,z}$	Reference
7.12	6.88	this work
7.21	6.87	Ref. 3
7.02	6.68	Ref. 4
7.13	6.72	Ref. 28
7.04	6.77	Ref. 29

TABLE IV. Calculated de Haas-van Alphen data of TaB_2.

orbit	F_{ASW} [KT]	F_{FPLO} [KT]	A_{ASW}/A_{BZ}	$m/m_\circ$	v_f [km/s]	$\tilde{v}_f$ [km/s]
1	2.08	2.50	0.041	0.221	1320	1410
2	2.99	3.48	0.059	0.356	979	1050
3	8.40	8.31	0.167	0.677	864	926
4	13.26	13.84	0.264	0.558	1320	1410
5	1.05	1.00	0.021	0.236	869	891
6	1.15	3.44	0.023	0.632	339	365

TABLE V. Squared plasma frequencies ω_{px}, ω_{pz}, and the anisotropy of averaged Fermi velocities for TaB_2 (in eV^2).

FS sheet	$\omega_{p,x(y)}$	$\omega_{p,z}$	$vx(y)/v_z$
1	68.125	84.779	0.90
2	15.149	17.049	0.94
3	3.243	3.254	1.00
All	86.52	105.08	0.91